Measurement of triplet exciton diffusion in organic light-emitting diodes

J. Wünsche,* S. Reineke, B. Lüssem, and K. Leo†
Institut für Angewandte Photophysik, George-Bähr-Strasse 1, D-01062 Dresden, Germany
(Received 1 March 2010; revised manuscript received 11 May 2010; published 4 June 2010)

A detailed investigation of the diffusion of triplet excitons in a layer of *N*,*N*′-di-1-naphthalenyl-*N*,*N*′-diphenyl-[1,1′:4′,1″:4″,1‴-quaterphenyl]-4,4‴-diamine (4P-NPD) incorporated in organic light-emitting diodes is presented. An appropriate method to measure the triplet diffusion length in fluorescent host materials is the spatial separation of the site of exciton generation from the site of radiative triplet decay by inserting a host spacer layer of varying thickness. However, cavity effects, the quenching and blocking of excitons at the boundaries of the spacer layer, and direct charge-carrier recombination in the sensing layer need to be taken into account. We use a specially designed layer stack, which excludes the influence of cavity effects on the measurements and a strongly quenching sensing layer, which ensures well-defined boundary conditions. The quenching of excitons by the sensing layer, the generation zone, and direct charge-carrier recombination are investigated experimentally and their influence on the extracted diffusion length are discussed. The significance of triplet-triplet annihilation in this analysis is estimated by a current-dependent evaluation. An analytic model for the dependence of the sensing layer emission on the spacer thickness is presented, which includes the important effects. By this means, we find a triplet diffusion length of 11 ± 3 nm in 4P-NPD.

DOI: 10.1103/PhysRevB.81.245201 PACS number(s): 71.35.Cc, 81.05.Fb, 85.60.Jb

I. INTRODUCTION

Organic light-emitting diodes (OLEDs) containing phosphorescent emitter materials can achieve close to 100% internal quantum efficiency since they can harvest singlet and triplet excitons for light emission due to strong spin-orbit coupling in phosphorescent molecules.[1] In contrast, fluorescent emitters are limited to 25% internal quantum efficiency since the radiative transition of triplets is forbidden due to spin conservation. After the first white OLEDs with fluorescent emitters,[2] also white OLEDs with three phosphorescent emitters doped into fluorescent host materials have been presented.[3,4] A balanced spectrum is achieved by controlling the energy transfer between separate emitting layers. Often, these OLEDs require a high operating voltage due to the wideband-gap host material used for the blue phosphor. However, it has been shown recently that the operating voltage can be reduced considerably by choosing a resonant blue guest-host system so that luminous efficacies are high.[5] Another approach is the combination of a fluorescent blue with two phosphorescent emitters, which promises higher device stability. In these devices, triplets created on the fluorescent emitter are transferred to spatially separated phosphorescent molecules. There, they can be harvested, allowing close to 100% internal quantum efficiency.[6,7] For both types of devices, the diffusion of triplet excitons plays a major role for efficiency and color balance. Meanwhile, in all OLEDs, diffusion to quenching sites reduces the efficiency. It is therefore of considerable interest to investigate the diffusion of triplets in host materials and determine the diffusion length.

Several methods have been suggested to analyze the diffusion of excitons. Well-established methods to determine the diffusion length of singlet excitons are, e.g., photocurrent measurements[8–11] and photoluminescence quenching experiments.[12–15] These methods are based on optical excitation and in the second case, also on radiative decay. For triplet excitons in fluorescent materials, these processes have very low transition moments. Therefore, these methods cannot be applied in its original form. Triplets can be excited indirectly by light with the help of a phosphorescent sensitizer[16] or by intersystem crossing.[17] However, since this involves additional states, these techniques require additional assumptions or complex time- and spectrally resolved studies, as presented by Giebink *et al.*[17] The absorption length for the excitation light is typically in the same order of magnitude as the triplet diffusion lengths or even larger and intersystem crossing rates are generally low in host materials, so one cannot expect to obtain always transients showing a clear sign of diffusion.

In contrast, when exciting the fluorescent host material electrically in an appropriate OLED structure, the exciton generation zone can be controlled to be thin and adjacent to either hole or electron blocking layer. From there, the triplets diffuse through the host layer, called spacer. They are detected by a phosphorescent sensing layer positioned at a defined distance from the generation zone. Another advantage of this method is that the conditions for exciton diffusion resemble much more those in real device structures, including all possible quenching mechanisms and a similar generation rate and zone. Baldo *et al.*[18] varied the thickness of a tris(8-hydroxyquinoline) aluminum (Alq_3) spacer and compared the emission of the sensing layer to determine the triplet diffusion length in Alq_3. They also analyzed the transient response of OLEDs incorporating spacer layers of different materials after applying a short voltage pulse.[19] They pointed out that delayed emission may result from triplet diffusion or charge-carrier movement. It was checked for the latter by applying a negative bias voltage after the pulse to remove free charge carriers. Although possibly yielding more information about diffusion, electroluminescent transient data need to be evaluated with care since the abrupt changes in the electrical field cause a significant movement of charges after the pulse, whose recombination superposes with the

emission resulting from exciton diffusion. Additionally, all time-dependent evaluations are complicated by the influence of the mostly unknown recombination velocity at the interface to the sensing layer.[20,21] Instead of varying the thickness of the spacer layer, D'Andrade *et al.*[3] varied the thickness of the phosphor-doped region. By this means, they obtained the transfer length of triplet excitons in *fac*-tris(2-phenylpyridine)iridium [$Ir(ppy)_3$] doped 4,4′-*N*,*N*′-dicarbozole-biphenyl (CBP) by comparing the device efficiencies. Their analysis was refined by Zhou *et al.*,[22] who presented a two-layer model which takes the influence of the sensing layer on the triplet diffusion into account. Thus, they were able to also extract the triplet diffusion length in pure CBP. Alternatively to thickness variations, it is also possible to incorporate a thin sensing layer at different positions inside the spacer, as proposed by Sun *et al.*[6] Choukri *et al.*[23] stressed that direct carrier recombination on the phosphor and cavity effects should be considered and obtained another value for the diffusion length in CBP. Recently, also Lebental *et al.*[24] discussed these aspects and investigated theoretically the influence of triplet-triplet annihilation (TTA) and of the sensing layer for the same method.

In this paper, we investigate the diffusion of triplet excitons in *N*,*N*′-di-1-naphthalenyl-*N*,*N*′-diphenyl-[1,1′:4′,1″:4″,1‴-quaterphenyl]-4,4‴-diamine (4P-NPD) based on the comparison of the spectra of OLEDs with different 4P-NPD-spacer thicknesses. 4P-NPD is a fluorescent blue host material with high photoluminescent yield and a high triplet energy and is therefore successfully used in high efficiency white OLEDs employing the triplet harvesting concept.[7] First, we introduce the device structure and state important material properties and experimental details in Sec. II. In Sec. III, the diffusion equation is solved with realistic boundary and initial conditions and the solution is related to the dependency of the sensing layer emission intensity on the spacer thickness. We investigate the generation zone and the influence of the sensing layer in Sec. IV to justify assumptions made and present the diffusion profile measured for different current densities together with the extracted diffusion length in Sec. V. The data are further analyzed with regard to direct carrier recombination and triplet-triplet annihilation in Sec. VI and conclusions are presented in Sec. VII.

II. EXPERIMENTAL METHOD

For our investigation, we use the approach of Baldo *et al.*[18] to vary the thickness of the spacer layer. It is less sensitive to deviations in the sensing layer thickness and concentration compared to the method of Sun *et al.*,[6] where a thin sensing layer is incorporated at different positions inside the spacer. An energy-level diagram of the devices fabricated to measure the triplet diffusion length, showing the highest occupied molecular orbitals and lowest unoccupied molecular orbitals (HOMOs and LUMOs, respectively), is shown in Fig. 1. They have a standard *p-i-n* structure, similar to the one in Ref. 7. *N*,*N*′-diphenyl-*N*,*N*′-bis(3-methylphenyl)-[1,1′-biphenyl]-4,4′-diamine (MeO-TPD) doped with

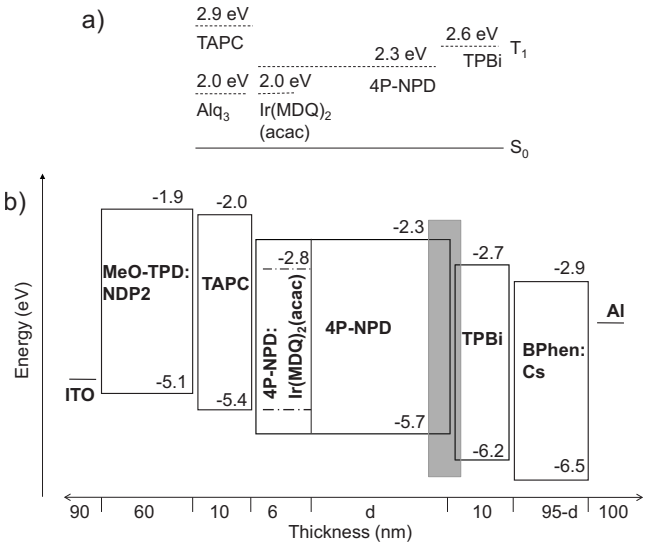

FIG. 1. (a) Triplet energies of selected materials used in this study. Alq_3 is used in Sec. IV to investigate the boundary conditions. (b) Schematic energy-level diagram of the devices fabricated to measure the diffusion length in 4P-NPD. Dashed-dotted lines: HOMO and LUMO of $Ir(MDQ)_2(acac)$.

NDP-2,[25] a proprietary *p* dopant from Novaled AG, Dresden, and Cs-doped 4,7-diphenyl-1,10-phenanthroline (BPhen) are used as hole and electron-transport layers, respectively. 10 nm of 1,1-bis(4-di-p-tolylaminophenyl)cyclohexan (TAPC) serve as electron blocking layer and 10 nm of 2,2′,2″(1,3,5-benzenetriyl)tris-[1-phenyl-1H-benzimidazole] (TPBi) as hole blocking layer. The emissive layer consists of a layer of pure 4P-NPD, called spacer, and the sensing layer, a 6-nm-thick layer of 4P-NPD doped with 5 wt % iridium(III)bis(2-methyldibenzo-[f,h]quinoxaline) (acetylacetonate) [$Ir(MDQ)_2(acac)$], a orange-red phosphorescent emitter. Indium tin oxide and aluminum are used as anode and cathode, respectively. The molecular structure and photoluminescence spectra of the emitting materials can be found in Fig. 2.

All samples are prepared on ITO-coated, structured glass substrates. Previous to the evaporation of the organic layers, they are cleaned in an ultrasonic bath with acetone, ethanol, and iso-propanol. The samples with a sensing layer of 4P-NPD:$Ir(MDQ)_2(acac)$ (0.5 wt%) (Sec. IV) are built in a high-vacuum multichamber tool (10^{-7} mbar). All other samples are prepared in a high-vacuum single-chamber tool (10^{-8} mbar). In both tools, all layers including the aluminum top contact are evaporated without breaking the vacuum. Immediately after preparation, the devices are encapsulated with epoxy glue and glass lids in a nitrogen atmosphere. The thicknesses of the evaporated layers are measured with independent quartz-crystal monitors. The density of 4P-NPD is determined more precisely with the help of x-ray reflectivity measurements after device preparation. All thicknesses of 4P-NPD layers are recalculated according to this value. The device area is 6.5 mm^2. Measurements of electroluminescent spectra and current-voltage characteristics are taken with a calibrated CAS140CT luminance meter from Instrument Systems and a Keithley SM2400 source-measure unit, re-

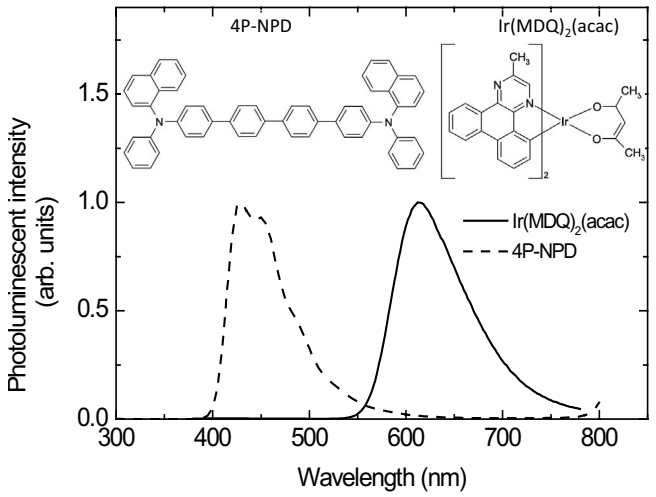

FIG. 2. Normalized photoluminescence spectra and molecular structures of 4P-NPD (bulk layer) and $Ir(MDQ)_2(acac)$ (doped with 20 wt % in NPD).

spectively. HOMO values are determined by ultraviolet photoelectron spectroscopy and LUMOs are estimated from the optical gap of the material or are taken from literature.[7,26–28] Photoluminescence spectra are recorded in a photo spectrometer (FluoroMax).

4P-NPD has good hole conducting properties,[7] whereas TPBi is an electron-transport material.[29] Furthermore both charge carriers are facing high energy barriers at the 4P-NPD/TPBi interface, about 0.5 eV for holes and 0.4 eV for electrons. It is therefore reasonable to assume that the charge-carrier recombination takes place close to this interface. The generation zone is investigated in Sec. IV. Singlet excitons created on 4P-NPD decay within a few nanometers,[30] whereas triplets are expected to diffuse a longer distance due to their longer lifetime. Hence, they can reach the sensing layer, where they can be harvested by $Ir(MDQ)_2(acac)$ molecules since their triplet energy is 0.3 eV below the one of 4P-NPD (see Fig. 1). This energy difference can be expected to be favorable for a fast energy transfer from 4P-NPD, according to Marcus theory. Furthermore, $Ir(MDQ)_2(acac)$ has a high photoluminescence yield.[26] Together with a sufficient doping concentration, this ensures that triplets reaching the sensing layer are transferred to $Ir(MDQ)_2(acac)$ within few nanometers. $Ir(MDQ)_2(acac)$ is well suited to quantify the number of triplets reaching the sensing layer since the peak of its emission spectrum has negligible overlap with the 4P-NPD spectrum (see Fig. 2).

The approach to use a strongly quenching sensing layer reflects the conditions in OLEDs designed for triplet harvesting. If this method is applied to investigate the triplet diffusion in these devices, the sensing layer is part of the real device boundary conditions and not an invasive probe layer. This is in contrast to the repositionable thin sensing layer method, where the sensing layer is chosen as a trade-off between its influence on the diffusion profile and sufficient light intensity. Lebental *et al.*[24] presented the theory to include the influence of the sensing layer in the calculation in this case. However, an additional parameter is necessary to describe this influence, which is also the case for the two-layer model of Zhou *et al.*[22] Neglecting the influence of the sensing layer meanwhile leads to an overestimation of the diffusion length, which is even larger if also samples with a spacer layer thinner than the diffusion length are evaluated.

The mechanism responsible for triplet diffusion is Dexter transfer. TAPC and TPBi effectively block 4P-NPD triplets due to their higher triplet energies of 2.9 eV and 2.6 eV, respectively.[31,32] The diffusion process competes with the nonradiative decay of triplets. Thus, the intensity of the phosphorescent emission from the sensing layer depends on the spacer thickness, which is varied between 12 and 77 nm in this study. For thicker 4P-NPD layers, the electron-transport layer is made accordingly thinner in order to keep the total thickness of the OLED and the position of the sensing layer constant. Thus, assuming similar refractive indices of all organic layers incorporated, the optical field remains unchanged in the sensing layer. This represents an advantage compared to previous investigations since cavity effects do not influence the measurements. These effects are usually either completely neglected or it is tried to minimize the error by shifting the sensing layer to the flat region of the optical field.[23,24] However, even in this way, the variation in the optical field introduces a considerable error since the diffusion profile is usually measured over several tens of nanometer.

III. THEORY

We investigate the diffusion of triplet excitons in the 4P-NPD spacer in steady-state operation of the devices described above. In one dimension, it is governed by the following differential equation:

$$D\frac{\partial^2 n(x)}{\partial x^2} - \frac{n(x)}{\tau} + G_0 e^{-x/g} = 0. \quad (1)$$

It consists of three terms, describing from left to right: the diffusive transport, the monomolecular decay of the excitation, and the generation of excitons. Here, $n(x)$ is the exciton density on 4P-NPD molecules, D the diffusion coefficient, τ the natural lifetime of the triplet excitons, G_0 the generation rate at $x=0$, and g the distance at which the generation rate decreases to $1/e$, i.e., the width of the generation zone. The distance x is measured from the interface 4P-NPD/TPBi. The diffusion is assumed to be homogenous and isotropic inside the spacer layer and the triplet exciton lifetime τ includes the radiative and nonradiative decay. Here, other quenching mechanisms like triplet-polaron or triplet-triplet annihilation are neglected. In Sec. VI, we show that they start to become significant only at very high current densities in these devices.

The investigation of the generation zone in Sec. IV confirms that exciton generation takes place close to the interface 4P-NPD/TPBi, as expected. It also reveals that despite the high energy barrier, there is a significant electron current through this interface. Thus, it is not reasonable to assume a delta-distributed generation zone, as is often done. To account for an extended generation zone, we introduced a generation term in Eq. (1). The exciton generation rate is proportional to the local carrier densities. It can therefore have a

very complex spatial distribution. In our device structure, holes accumulate at the interface 4P-NPD/TPBi. As the simplest assumption, we choose an exponential decrease in the generation rate with the distance from this interface. The same assumption was made, e.g., in Ref. 19 and similar dependencies have been found in Refs. 33 and 34. Even though the real spatial distribution of the generation rate will deviate from this, it is a better approximation than the commonly assumed delta distribution at the interface. Accounting for an extended generation zone allows to apply the presented model also to OLED structures that might have a less confined generation zone without risking the overestimation of the diffusion length.

To obtain a realistic diffusion profile, it is also important to choose boundary conditions which are close to those in real device structures. In the OLEDs described in the previous section, TPBi effectively blocks the triplet excitons due to its high triplet energy. This implies that the exciton current through this interface is zero, i.e.,

$$\frac{\partial n(0)}{\partial x} = 0. \tag{2}$$

On the opposite side, the influence of the sensing layer on the triplet exciton distribution has to be considered. It can be described by introducing the capture parameter k as the proportionality constant between the spatial derivative of the triplet exciton density at this interface to the sensing layer and the density itself.[20,21] It is a measure for the transfer rate from 4P-NPD to $Ir(MDQ)_2(acac)$ at the interface. The second boundary condition reads then

$$\frac{\partial n(d)}{\partial x} = -kn(d), \tag{3}$$

where d is the thickness of the spacer layer. If the triplet exciton density inside the sensing layer is approximated as exponentially decreasing, $1/k$ can be thought of as a capture length within which all but $1/e$ of the triplets are transferred to $Ir(MDQ)_2(acac)$. To avoid this additional parameter, a sensing layer is chosen that captures all arriving triplets within few nanometers. In Sec. IV, data will be presented which confirm this assumption. In this range, k has no significant influence on the extracted diffusion length. Therefore, the interface of spacer and sensing layer can be approximated as perfectly quenching, which yields the second boundary condition,

$$n(d) = 0. \tag{4}$$

For the analysis in this work, the definition $L = \sqrt{D\tau}$ is used for the diffusion length. Since the diffusion profile deviates from the monoexponential decay because of the given generation term and boundary conditions, L no longer equals exactly to the length over which the triplet density drops to $1/e$. Often, the expression "effective triplet diffusion length" is used when the diffusion length is reduced by triplet-triplet annihilation at high current densities but yet this quenching mechanism is not included in the calculation. This quantity allows to estimate how far triplets diffuse under these conditions but is not well defined.

The solution of Eq. (1) is

$$n(x) = \frac{gG_0\tau}{L^2 - g^2}\left(2\frac{Le^{d/L} + ge^{-d/g}}{e^{d/L} + e^{-d/L}}\cosh\frac{x}{L} - Le^{x/L} - ge^{-x/g}\right). \tag{5}$$

In Sec. V, we evaluate the intensity of the phosphorescent emission from the sensing layer at constant current densities for different spacer thicknesses. Since the number of injected charge carriers is constant, the number of emitted photons from the sensing layer is proportional to the external phosphorescent quantum efficiency,

$$\eta_{ext} = \eta_c \beta \phi_{PL} \chi, \tag{6}$$

where η_c is the charge balance factor, β the ratio of generated excitons ending up in an emissive triplet state, ϕ_{PL} the photoluminescence quantum yield, and χ the outcoupling efficiency for the sensing layer. Assuming that the variation in the spacer thickness has no influence on the generation zone and that different current densities result only in different generation rates G_0 but not in a broadening or shift of the generation zone, η_c is constant. These two conditions will be investigated in Sec. IV. Furthermore, χ is the same for all devices since the sensing layer remains at the same position inside the cavity. Hence, the only quantity influenced by the spacer thickness is β. To relate β to the triplet distribution, some further assumptions need to be made. First, direct carrier recombination in the sensing layer is excluded for the moment and will be added later on. Furthermore, all triplets reaching the sensing layer are assumed to be transferred to $Ir(MDQ)_2(acac)$ molecules, where a constant ratio decays radiatively. Then, β and thus also the intensity of the phosphorescent sensing layer emission is proportional to the triplet exciton current into the sensing layer,

$$j(d) = -D\frac{\partial n(d)}{\partial x}. \tag{7}$$

Hence, the fit function of the diffusion profile is proportional to the spatial derivative of the exciton distribution, given by Eq. (5). Additionally, a term B is added for the contribution from direct charge-carrier recombination in the sensing layer, which will be motivated in the following section. It is constant for all spacer thicknesses. The resulting function used to fit the measured dependency of the sensing layer emission on the spacer thickness reads then

$$I(d) = -A\left[\left(e^{d/L} + \frac{g}{L}e^{-d/L}\right)\tanh\frac{d}{L} - e^{d/L} + e^{-d/g}\right] + B, \tag{8}$$

where I is the electroluminescent intensity and A is a proportional factor including the first factor in $n(x)$, Eq. (5), the diffusion coefficient and the radiative and outcoupling efficiencies for $Ir(MDQ)_2(acac)$. Figure 3 illustrates the deviation of the fit function from a monoexponential decrease. It can be seen that the introduction of blocking and quenching boundaries and a generation zone with an extent of about up to a third of the diffusion length effects the diffusion profile mainly within the first diffusion length. On the other side, direct charge-carrier recombination can change significantly the slope for larger spacer thicknesses. However, if the width

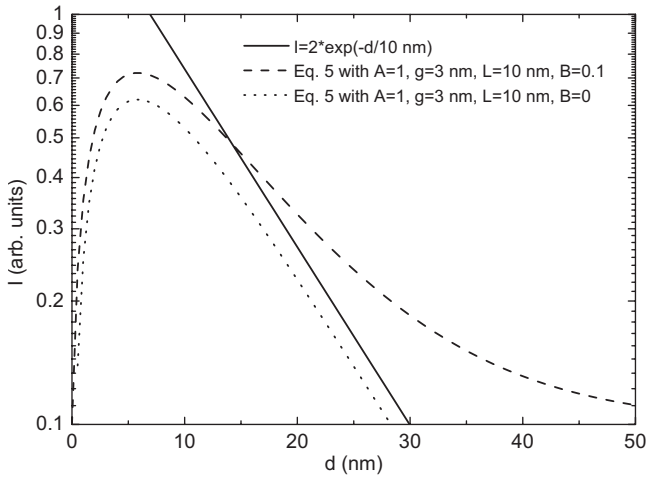

FIG. 3. Simulated diffusion profiles according to Eq. (8) with (dashed line) and without (dotted line) direct carrier recombination. The parameters are given in the legend. For comparison, the solid line shows a monoexponential decrease for the same diffusion length.

of the generation zone and the diffusion length are in the same order of magnitude, their influences on the diffusion profile are difficult to distinguish. The assumption of a too thin generation zone leads then to the overestimation of the diffusion length.

IV. GENERATION ZONE AND THE INFLUENCE OF THE SENSING LAYER

Since the generation zone has an influence on the diffusion profile, as discussed in the previous section and as becomes apparent from Eq. (8), its investigation is important to obtain exact results for the diffusion length. In particular, it has to be verified that the generation zone does not change for the different spacer thicknesses and current densities used for the study.

The generation zone is the site of exciton creation. It has to be distinguished from the emission zone, where excitons decay radiatively after possible Förster and Dexter transfers. It is not straightforward to measure the generation zone since any measured singlet or triplet profile includes these transfers. Since singlets have a much shorter lifetime than triplets, they are expected to diffuse a shorter distance before decay. Thus, measuring the singlet profile with a thin repositionable fluorescent sensing layer inside the 4P-NPD-spacer layer helps to better estimate the extension of the generation zone. However, the singlet diffusion length in (α-NPD), a material differing only in two phenyl rings from 4P-NPD and having similar properties,[7] was found to be (5.1 ± 1.0) nm by Lunt *et al.*[12] and the Förster radius of the transfer to the fluorescent sensing layer might be in the range of a few nanometer as well. Therefore, the measured profile is considerably smeared out compared to the real generation zone. It is thus not possible to extract the exact thickness of the recombination zone but rather its position and any possible changes due to spacer thickness or current variations.

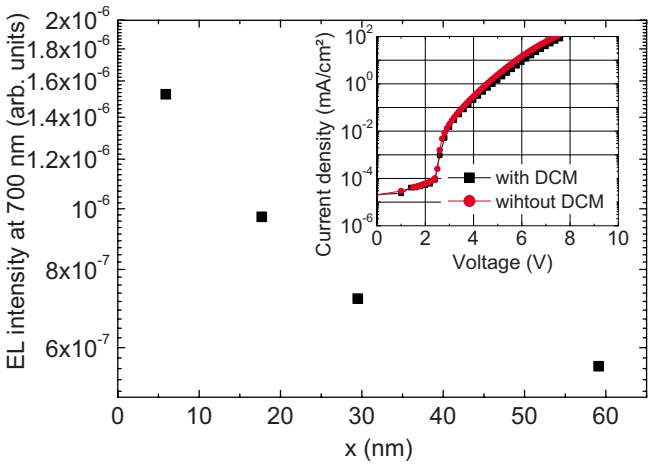

FIG. 4. (Color online) DCM emission intensity vs the distance x of the fluorescent sensing layer from the hole blocking layer. The inset shows the current-voltage characteristics for two samples with the same layer structure, one with DCM (squares) and one without (circles).

We use a 1-nm-thin sensing layer of 4-dicyanomethylene-2-methyl-6-p-dimethylaminostyryl-4H-pyran (DCM) at different positions inside a 59 nm spacer layer. DCM is chosen because it is an efficient fluorescent emitter whose emission (peak around 650 nm in electroluminescence) can be easily distinguished from that of 4P-NPD. The rest of the stack equals the one presented in Sec. II except for the phosphorescent sensing layer, which is substituted by additional 6 nm of pure 4P-NPD here. Furthermore, the thicknesses of the transport layers are adjusted to keep DCM at the same position inside the cavity. The intensity of the DCM emission is evaluated at a wavelength of 700 nm, where the overlap with the 4P-NPD spectrum is negligible. Figure 4 shows these intensities for a current density of 77.0 $\mathrm{mA/cm^2}$ plotted versus the position x of the sensing layer, as measured from the TPBi interface. The inset shows the current-voltage characteristics for two samples with 59 nm spacer. Their layer structure is identical except for the DCM layer which is incorporated only in one of the two devices at $x=59$ nm. The current-voltage behavior is very similar so that the influence of DCM on the electrical behavior can be neglected. The current-voltage characteristics are equally independent from the position of the DCM layer.

From the plot of the DCM intensity versus its position, it can be seen that the generation zone is located at the interface of 4P-NPD and TPBi, as expected. However, even at 59 nm distance from the 4P-NPD/TPBi interface, there is still a considerable emission from DCM observable. It is unlikely that the emission at 59 nm follows from singlet diffusion from the generation zone to the sensing layer. Thus, there has to be a non-negligible current of electrons through the 4P-NPD/TPBi interface, which results in direct carrier recombination on the DCM molecules. Together with the fact that phosphorescent emitters doped in host materials tend to trap holes effectively,[35] this suggests direct carrier recombination in the phosphorescent sensing layer as well. The rate of direct recombination is expected to be constant for all spacer thicknesses, leading to a plateau of sensing layer emission at

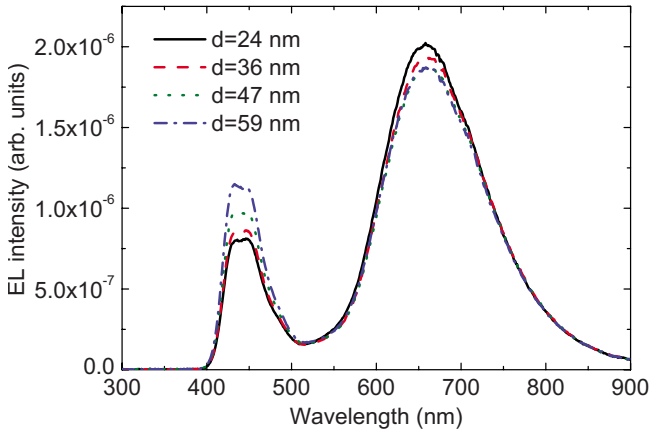

FIG. 5. (Color online) Electroluminescence spectra of the devices with DCM sensing layer at 15 nm from the interface to TPBi. The spacer thickness d varies from 24 to 59 nm.

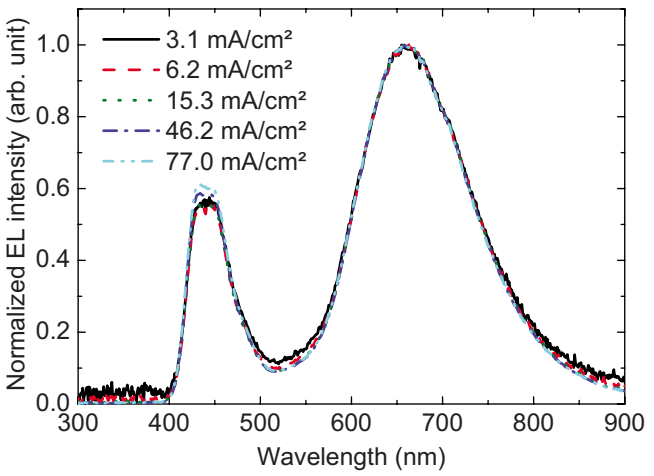

FIG. 6. (Color online) Electroluminescence spectra of the devices with DCM sensing layer at 18 nm from the interface to TPBi and a spacer thickness of $d=53$ nm for different current densities.

high thicknesses. It is included in the fit function [Eq. (8)] by the fit parameter B, which depends on the current but is independent of d. The necessity of considering direct carrier recombination was also stressed in other works.[23,24] Additionally, the electron current beyond the interface 4P-NPD/TPBi points to an extended generation zone of a width of few nanometer rather than a delta-distributed one.

The use of a fluorescent sensing layer to measure direct carrier recombination has been proposed before.[23,24] This technique is well suited to check for electron or hole currents in the emitting layer beyond the generation zone, which are necessary to obtain direct carrier recombination. However, it does not allow to quantify the importance of the latter in the diffusion experiment since the ability of charge trapping might be quite different on the fluorescent and phosphorescent sensor. Since electron and hole currents beyond the generation zone can rarely be excluded in typical device structures for this method, direct carrier recombination should always be considered in the analysis. Otherwise, the diffusion length can be severely overestimated.

Figure 5 plots the spectra at a current density of 77.0 mA/cm^2 for devices with 24, 36, 47, and 59 nm spacer layers. In all cases, DCM is located at 6 nm from the interface to TPBi. Cavity effects on the DCM emission are again excluded by adjusting the transport layers. In case of shifting toward the sensing layer or broadening of the generation zone for different spacer thicknesses, we would expect a higher emission from DCM. However, Fig. 5 shows that for increasing spacer thickness, the DCM intensity decreases slightly, whereas there is a more pronounced increase in 4P-NPD emission. The same behavior, but with much smaller differences in DCM emission, is observed for devices with DCM positioned at 18 nm from TPBi. Small changes can be explained by unwanted thickness and resulting cavity variations, whereas the systematic increase in 4P-NPD emission seems to indicate a different process. We suggest that with increasing spacer thickness, the bulk recombination on 4P-NPD rises. That means, a larger number of excitons might be formed well behind the sensing layer in the bulk and therefore fewer excitons at the interface to TPBi, resulting in less emission from DCM. A DCM layer more centrally located can harvest more of the excitons generated in the bulk and consequently shows a lower decrease in emission. Due to the changed distribution of excitons, the 4P-NPD emission is now influenced by cavity effects, possibly increasing the outcoupling efficiency. It should be noted, however, that the observed changes in Ir(MDQ)$_2$(acac) emission are relatively small even for the large variation in spacer thickness in this work and that the introduced error is in the same range as the one resulting from thickness deviations between the samples and the unknown extent of the generation zone.

The independence of the shape of the generation zone from the applied current can be seen in Fig. 6, which plots the normalized spectra of the device with DCM at $x=18$ nm in a spacer layer of 53 nm for current densities between 1.5 and 77.0 mA/cm^2. Deviations occur only at the highest current densities and are within the range of error. Therefore, we conclude that the generation zone remains unchanged for different current densities.

In summary, the influence of current and spacer thickness on the site of exciton generation has been found to be negligible in the devices presented here, which is an important condition for the evaluation of the diffusion profile in Sec. V.

In Sec. III, we made the assumption of a perfectly quenching interface between the spacer and sensing layer, motivated by using a phosphorescent emitter known to be efficient when doped into α-NPD.[7,26] To verify this assumption, devices equal to those introduced in Sec. II but with 5 wt % Alq$_3$ doped electron blocking layer [TAPC, $E_T=2.9$ eV (Ref. 31)] are prepared. The fluorescent green emitter Alq$_3$ has a triplet energy of 2.0 eV.[36] Consequently, 4P-NPD triplets reaching the electron blocking layer should be transferred to the nonemissive triplet state of Alq$_3$, where they are lost for emission since the back transfer to 4P-NPD is unlikely due to its higher triplet energy. Thus, if a detectable amount of triplets is not transferred to Ir(MDQ)$_2$(acac) within the 6-nm-thick sensing layer but reaches the blocking layer, a lower emission from Ir(MDQ)$_2$(acac) should result. In Fig. 7, the emission spectra for different spacer thicknesses with and without Alq$_3$ are shown.

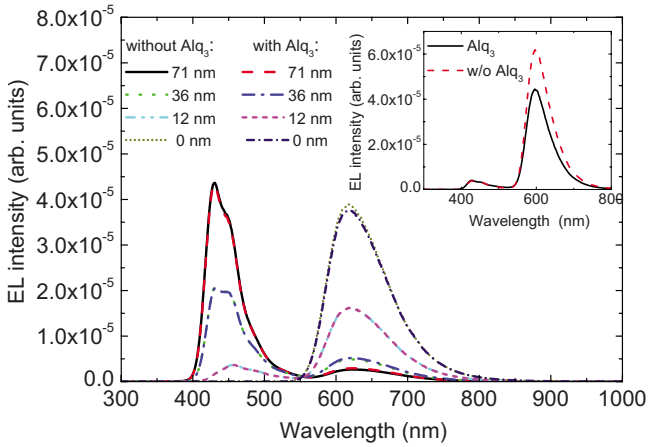

FIG. 7. (Color online) Electroluminescence spectra at a current density of 77 mA/cm^2 for four different spacer thicknesses d with and without Alq_3 doped in the electron blocking layer. All but those for $d=0$ remain unchanged. The inset shows the spectra of two reference samples with $d=0$ and only 0.5 wt % $Ir(MDQ)_2$.

The spectra are plotted for the samples with doped and undoped blocking layer and are obtained at a current density of $j=77$ mA/cm^2, which corresponds to the highest current density used to determine the diffusion length in Sec. V. Only if the spacer layer is omitted, which corresponds to high triplet densities in the sensing layer, a small decrease in emission can be seen. The emission from 4P-NPD and also the current-voltage characteristics remain unchanged. To prove the principle of quenching by Alq_3, two additional samples are prepared (in UFO2) with a less effective sensing layer. This is achieved by lowering the concentration of $Ir(MDQ)_2(acac)$ to 0.5 wt %. In one sample, the electron blocker is doped with Alq_3 and in the other, it remains undoped. From the spectra in the inset of Fig. 7, it can be seen that almost a third of the $Ir(MDQ)_2(acac)$ emission is quenched by Alq_3. Therefore, we conclude that a sensing layer doped with 5 wt % $Ir(MDQ)_2(acac)$ is sufficient to capture the vast majority of triplet excitons within 6 nm. Because of the unknown sensitivity of the quenching by Alq_3 and its unknown influence on the triplet distribution, it is not possible to quantify the capture parameter k introduced in Sec. III. However, it can be estimated that k is well above 0.17 nm^{-1}, which corresponds to a capture length of 6 nm. Figure 8 shows some simulated diffusion profiles with $g=3$ nm, $L=10$ nm, and k ranging from 0.01 to 1 nm^{-1}. In this range, the influence of k on the diffusion profile is restricted to the region within one diffusion length, where no data points are used for fitting. Thus, the boundary condition $n(d)=0$ is a reasonable approximation.

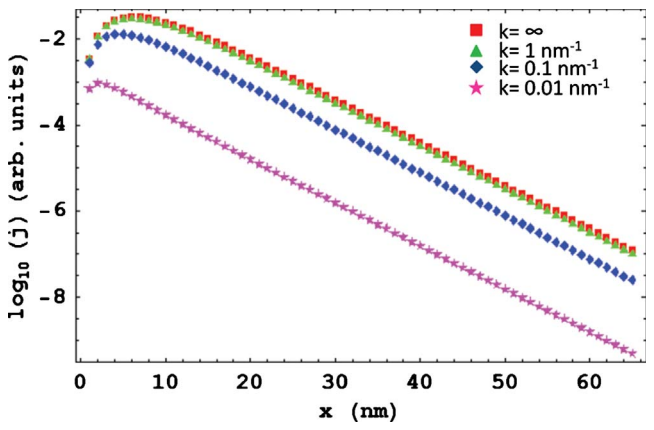

FIG. 8. (Color online) Simulated triplet currents into the sensing layer, which are proportional to the measured diffusion profile, for $g=3$ nm, $L=10$ nm, and k ranging from 0.01 to 1 nm^{-1}. Direct recombination processes are not considered. k has no influence on the extracted diffusion length, which is obtained by fitting the data at $x>18$ nm and does not depend on the absolute intensity.

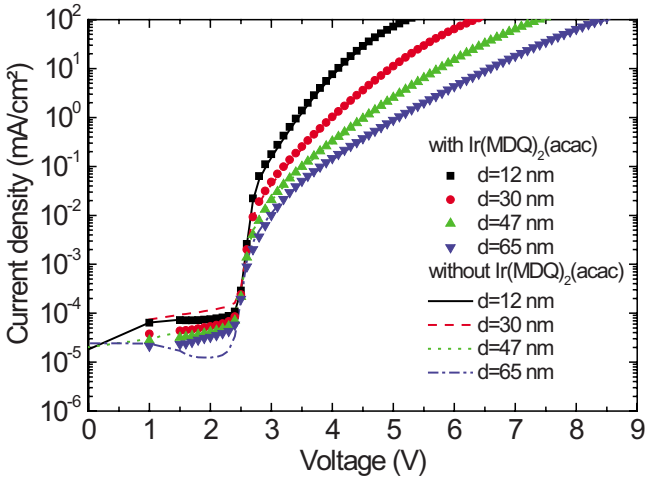

FIG. 9. (Color online) Current voltage characteristics for different spacer thicknesses with (symbols) and without (lines) $Ir(MDQ)_2(acac)$.

V. TRIPLET DIFFUSION LENGTH IN 4P-NPD

Figure 9 shows the current-voltage characteristics of four devices of the set of OLEDs presented in Sec. II and their reference devices without $Ir(MDQ)_2(acac)$. The presence of the phosphor has no measurable influence on the electrical

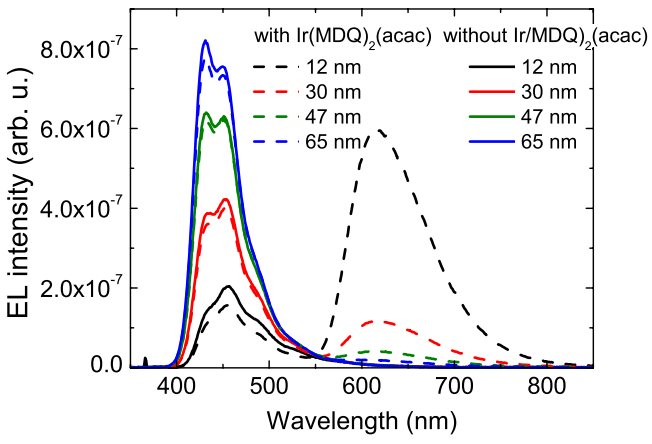

FIG. 10. (Color online) Electroluminescent spectra for different spacer thicknesses with (dashed lines) and without (lines) $Ir(MDQ)_2(acac)$.

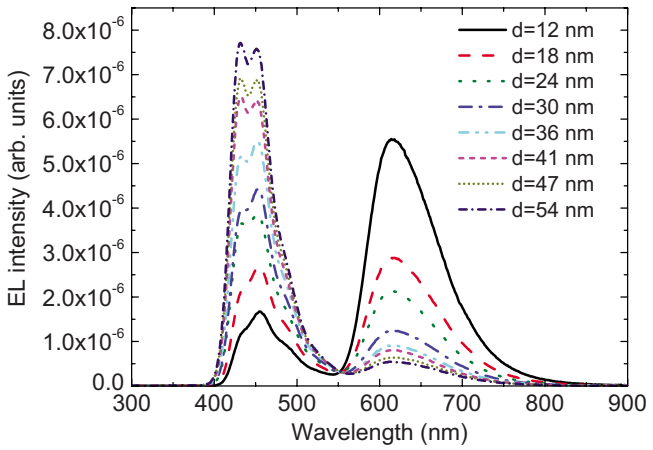

FIG. 11. (Color online) Electroluminescence spectra of the devices described in Sec. II for different 4P-NPD-spacer thicknesses, measured at a current density of 15.4 mA/cm^2.

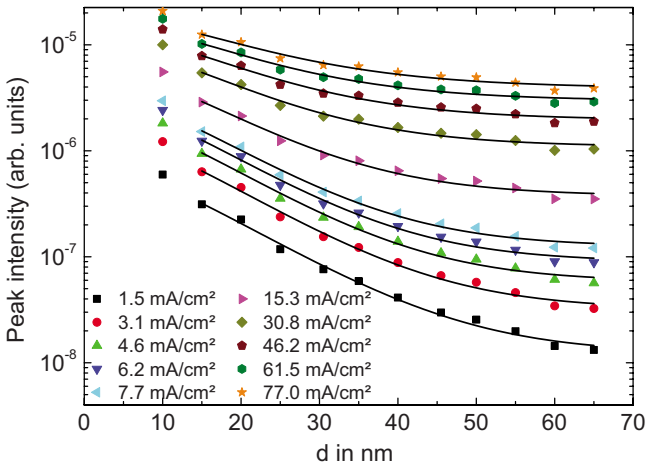

FIG. 12. (Color online) Peak intensity of $Ir(MDQ)_2(acac)$ vs the spacer thickness for different current densities (symbols). The lines correspond to the fit by Eq. (8).

behavior. The resistance of the devices increases with increasing thickness of the 4P-NPD spacer, as expected due to the small carrier mobilities in intrinsic layers.

The spectra for the devices with and without sensing layer are compared in Fig. 10. The reference devices without $Ir(MDQ)_2(acac)$ show the same intensities of 4P-NPD emission within experimental error and the same changes with the spacer thickness. This confirms that there is no significant Förster transfer of singlets from 4P-NPD to $Ir(MDQ)_2(acac)$. The relative difference in the 4P-NPD peak height is slightly larger for the devices with only 12 nm spacer layer. They are therefore excluded for the fit.

Figure 11 shows the spectra of all samples with sensing layer at a current density of 15.4 mA/cm^2. The intensity and the shape of the 4P-NPD peaks (around 430 and 450 nm) change due to cavity effects. The sensing layer, however, has always the same position in the cavity. The height of the $Ir(MDQ)_2(acac)$ peak (around 620 nm) changes due to the varying distance that triplet excitons have to diffuse prior to decay in the sensing layer. Since the shape of the peak is the same for all devices and the contribution of 4P-NPD to the spectra at this wavelength is negligible, we can directly evaluate the peak intensities of $Ir(MDQ)_2(acac)$.

Figure 12 shows the $Ir(MDQ)_2(acac)$ peak intensities plotted versus the thickness of the spacer layer for different current densities. The diffusion profile differs significantly from a monoexponential decay, mainly due to direct charge-carrier recombination processes. The data are fitted according to Eq. (8). The parameter g, representing the thickness of the generation zone, cannot be used as a free parameter in this fit since its influence on the diffusion profile is only visible within the first nanometers, where no data points are taken since direct Förster transfer from 4P-NPD to $Ir(MDQ)_2(acac)$ is likely to superpose the diffusion profile there. Reasonable fits can be obtained for g between 0 and 7 nm. Values of up to 4 nm yield diffusion lengths from 11 nm for low currents to 15 nm for the highest currents. The assumption of a thicker generation zone leads to reduced values for the diffusion length, e.g., by two nanometers in case of a 7-nm-thick generation zone. Since the lower values for g yield slightly better fits, g is fixed to 3 nm in this analysis. The fits shown in Fig. 12 are obtained by not considering the data point at $d=11$ nm, where a contribution from singlet diffusion and Förster transfer to the population of the triplet state of $Ir(MDQ)_2(acac)$ is likely, as is also suggested by the singlet emission profile in Fig. 4. Additionally, the influence of triplet-triplet annihilation is stronger in this region of high triplet densities.

Table I summarizes the fit results. Except for very high currents, a diffusion length of (11 ± 3) nm is obtained. The error is estimated from uncertainties arising from thickness variations in the evaporated layers, the unknown extent of the generation zone and its possible small changes. The current dependence will be discussed in the following section. A comparison to other materials is difficult since the triplet diffusion length tends to vary over several orders of magnitude depending on material, morphology, and impurities. However, the value obtained in this work is in good agreement with the diffusion length found for α-NPD in photocurrent experiments by Luhman and Holmes,[16] (11.8 ± 0.6) nm.

TABLE I. Fit parameters for the diffusion profile in Fig. 12 for different current densities j according to Eq. (8). A is the intensity of the sensing layer emission resulting from triplet diffusion and B the intensity from direct charge-carrier recombination. L is the diffusion length. The width of the generation zone g is fixed to 3 nm for the calculated fits.

j (mA/cm^2)	1.5	3.1	4.6	6.2	7.7	15.4	30.8	46.2	61.5	77.0
L (nm)	11.4	11.2	11.1	11.0	11.1	11.6	12.5	13.3	13.9	14.7
A (10^{-6}) arb. units	0.91	1.88	2.79	3.67	4.38	7.32	11.29	13.93	16.18	17.81
B (10^{-6}) arb. units	0.01	0.03	0.06	0.10	0.13	0.39	1.12	1.99	3.01	3.96

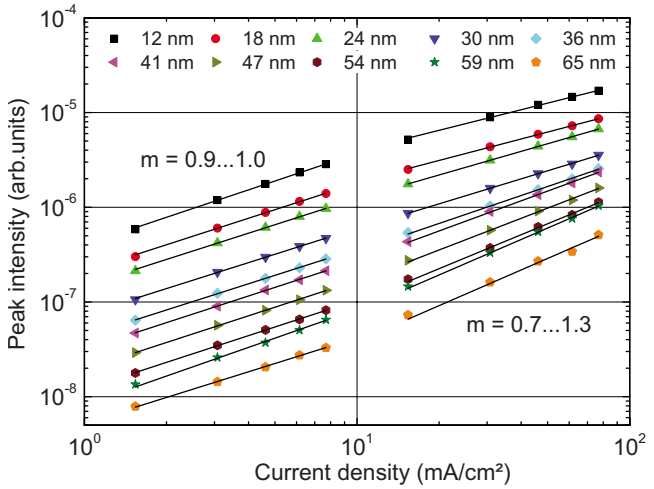

FIG. 13. (Color online) Double-logarithmic plot of the $Ir(MDQ)_2(acac)$ peak intensity I vs the current densities j for different spacer thicknesses. The lines refer to fits with the function $I=aj^m$.

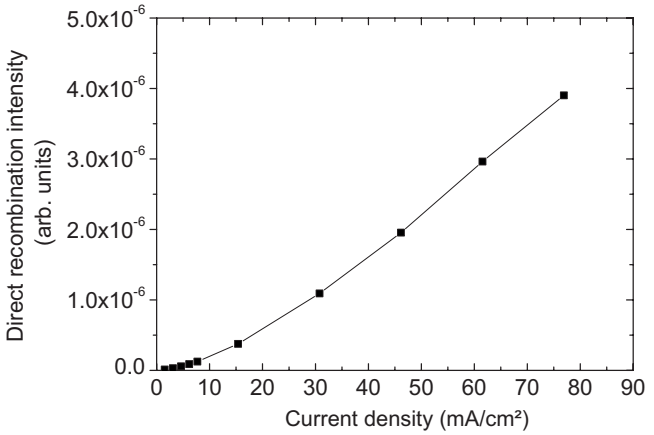

FIG. 14. Intensity of direct recombination vs the current density, according to the fit results in Table I.

In their experiment, almost 100% of the excitation energy was transferred to the α-NPD triplet state with the help of a phosphorescent sensitizer. The triplet diffusion length measured exceeds that for singlet excitons in α-NPD (Ref. 12) only by a factor of 2. The effect of a lifetime being several orders of magnitude higher than the one of singlet excitons seems to be compensated by a much smaller diffusion coefficient in the case of triplets. Unlike singlets, which can be transferred by long-range Förster transfer, triplets on host materials can migrate only by the short-range Dexter transfer.

VI. TRIPLET-TRIPLET ANNIHILATION AND DIRECT RECOMBINATION

In the model employed, the diffusion length should be independent of the current density. Up to 15.4 mA/cm^2, the fit indeed yields an almost constant value of 11 nm. However, it increases slightly up to 15 nm for the highest current densities (see Table I). This is an interesting effect, since one would expect the diffusion length to decrease at high current densities because of triplet-polaron annihilation (TPA) and TTA, which have not been considered in the model.

Figure 13 is a double-logarithmic plot of the peak intensities for different spacer thicknesses versus the current densities. The contribution from direct charge-carrier recombination is subtracted before.

In the case that only the monomolecular decay is significant, the intensity would rise linearly, resulting in a slope of $m=1$. If TPA and/or TTA were the dominating decay processes, the intensity would be proportional to the square root of the current density.[37] This corresponds to a slope of $m=0.5$. The double-logarithmic plot is therefore a good measure to verify the validity of the applied model. A linear fit in the plot for current densities from 1.5 to 7.7 mA/cm^2 yields slopes of 0.9–1.0. However, for higher current densities, the slope varies from 0.7 for $d=12$ nm to 1.3 for $d=65$ nm. The slopes smaller than one point to a slowly growing importance of TTA. Understandably, this effect is stronger for the thinner spacer layers, where the average triplet density is higher. The superlinear behavior for thicker spacer layers is surprising. It corresponds to the higher diffusion lengths obtained for high current densities. One possible reason, a shift of the generation zone was ruled out in Sec. IV. Although no final explanation can be given at this point, we have some suggestions to explain this behavior. For charge carriers, it is known that the mobility and therefore also the diffusion coefficient increases with increasing carrier density.[38,39] Assuming that there is an energetic distribution of triplet substates, a similar dependence might be possible for the diffusion of excitons. This might be measurable at exciton densities where bimolecular quenching does not yet dominate. We have also recently obtained preliminary results which suggest that the current dependence and the diffusion length itself can be influenced by the 4P-NPD layer morphology. Comparing the values for A and B in Table I, it can be seen that the direct recombination of charge carriers in the sensing layer plays indeed an important role in these devices, as expected from the electron current found in the emitting layer by the investigation described in Sec. IV. In Fig. 14, B is plotted as a function of the current density j. It increases linearly with j, indicating that direct recombination in the sensing layer is rather limited by the current than by the concentration of phosphorescent molecules. In fact, at high currents and large spacer thicknesses, direct carrier recombination contributes more to the sensing layer emission than triplet diffusion (as can be seen from comparison of Figs. 13 and 14). The higher diffusion lengths obtained for high current densities might therefore also be caused by the fit procedure. Further investigations will be needed to confirm one of the possible explanations. However, we note that the model employed gives consistent results for current densities up to 15 mA/cm^2 and fits perfectly the data obtained.

VII. CONCLUSIONS

We present a thorough analysis of the diffusion of triplet excitons in OLEDs under steady-state operation. For this in-

vestigation, the emitting layer of the OLEDs consists of a layer of the host material, the spacer, and a thin phosphorescent sensing layer. The OLED architecture for this method is improved in two aspects. Cavity effects due to different positions of the sensing layer, which were often superposing the exciton distribution in previous studies, can be excluded by adjusting the thicknesses of the transport layers. The usage of an effective sensing layer, approximated as perfectly quenching, allows both spectra of high intensity and defined boundary conditions without introducing new parameters.

With a fluorescent sensing layer (DCM), we investigate direct charge-carrier recombination in the sensing layer and possible changes in the position and width of the generation zone. Uncertainties of this method are also discussed. By this means, we find a current of electrons through the interface of TPBi and 4P-NPD. A current-dependent evaluation allows us to estimate that the influence of triplet-triplet annihilation becomes significant only at the highest current densities and by the spectral analysis of additional devices with an Alq_3 doped electron blocking layer, we can justify the boundary condition of a perfectly quenching sensing layer. The presented analytical model is based on this boundary condition, an extended generation zone, and the possibility of direct charge carriers recombination. In this way, a triplet diffusion length of (11 ± 3) nm in 4P-NPD is found. Despite the much longer lifetime of triplets, this value has the same order of magnitude as typical diffusion lengths for singlet excitons,[12] implying that the diffusion coefficient for triplets is much smaller due to the short range of Dexter transfer.

Finally, we note that this method can be well applied to measure the diffusion length in other materials. However, an appropriate layer stack need to be found to ensure that the generation zone is adjacent to one of the blocking layers and does not change for different spacer thicknesses or currents. In future works, the model should additionally include nonlinear decreases at high excitation levels, at best with experimental determination of the corresponding rates.

ACKNOWLEDGMENTS

The authors thank M. Hoffmann for fruitful discussions. The work leading to these results has received funding from the European Community's Seventh Framework Programme under grant Agreement No. FP7–224122 (OLED100.eu).

*Present address: École Polytechnique de Montréal, Département de génie physique, 2900, boul. Édouard-Montpetit, Campus de l'Université de Montréal, 2500, chemin de Polytechnique, Montréal (Québec), Canada H3T 1J4.

†leo@iapp.de

[1] M. Baldo, D. O'Brien, Y. You, S. Shoustikov, S. Sibley, M. Thompson, and S. Forrest, Nature (London) **395**, 151 (1998).

[2] K. N. J. Kido and M. Kimura, Science **267**, 1332 (1995).

[3] B. D'Andrade, M. Thompson, and S. Forrest, Adv. Mater. **14**, 147 (2002).

[4] Y. Sun and S. R. Forrest, Appl. Phys. Lett. **91**, 263503 (2007).

[5] S. Reineke, F. Lindner, G. Schwartz, N. Seidler, K. Walzer, B. Lüssem, and K. Leo, Nature (London) **459**, 234 (2009).

[6] Y. Sun, N. C. Giebink, H. Kanno, B. Ma, M. E. Thompson, and S. R. Forrest, Nature (London) **440**, 908 (2006).

[7] G. Schwartz, M. Pfeiffer, S. Reineke, K. Walzer, and K. Leo, Adv. Mater. **19**, 3672 (2007).

[8] A. K. Ghosh and T. Feng, J. Appl. Phys. **49**, 5982 (1978).

[9] S. Banerjee, A. P. Parhi, S. S. K. Iyer, and S. Kumar, Appl. Phys. Lett. **94**, 223303 (2009).

[10] H. Gommans, S. Schol, A. Kadashchuk, P. Heremans, and S. Meskers, J. Phys. Chem. C **113**, 2974 (2009).

[11] J. Kalinowski and K. Szybowska, Org. Electron. **9**, 1032 (2008).

[12] R. R. Lunt, N. C. Giebink, A. A. Belak, J. B. Benziger, and S. R. Forrest, J. Appl. Phys. **105**, 053711 (2009).

[13] S. R. Scully and M. D. McGehee, J. Appl. Phys. **100**, 034907 (2006).

[14] A. Holzhey, C. Uhrich, E. Brier, E. Reinhold, P. Bäuerle, K. Leo, and M. Hoffmann, J. Appl. Phys. **104**, 064510 (2008).

[15] J. Kalinowski, V. Fattori, and P. Marco, Chem. Phys. **266**, 85 (2001).

[16] W. A. Luhman and R. J. Holmes, Appl. Phys. Lett. **94**, 153304 (2009).

[17] N. Giebink, Y. Sun, and S. Forrest, Org. Electron. **7**, 375 (2006).

[18] M. A. Baldo, D. F. O'Brien, M. E. Thompson, and S. R. Forrest, Phys. Rev. B **60**, 14422 (1999).

[19] M. A. Baldo and S. R. Forrest, Phys. Rev. B **62**, 10958 (2000).

[20] B. A. Gregg, J. Sprague, and M. W. Peterson, J. Phys. Chem. B **101**, 5362 (1997).

[21] R. Schüppel, T. Dienel, K. Leo, and M. Hoffmann, J. Lumin. **110**, 309 (2004).

[22] Y. C. Zhou, L. L. Ma, J. Zhou, X. M. Ding, and X. Y. Hou, Phys. Rev. B **75**, 132202 (2007).

[23] H. Choukri, M. Lebental, S. Forget, S. Chénais, D. Adès, A. Siove, and B. Geffroy, Proc. SPIE **6999**, 699908 (2008).

[24] M. Lebental, H. Choukri, S. Chénais, S. Forget, A. Siove, B. Geffroy, and E. Tutis, Phys. Rev. B **79**, 165318 (2009).

[25] NDP-2 has similar electrical properties as 2,3,5,6-tetrafluoro-7,7,8,8-tetracyanoquinodimethane (F4-TCNQ) but is chosen for reasons of better processing.

[26] R. Meerheim, S. Scholz, S. Olthof, G. Schwartz, S. Reineke, K. Walzer, and K. Leo, J. Appl. Phys. **104**, 014510 (2008).

[27] L.-B. Lin, R. H. Young, M. G. Mason, S. A. Jenekhe, and P. M. Borsenberger, Appl. Phys. Lett. **72**, 864 (1998).

[28] J. Kalinowski, M. Cocchi, D. Virgili, V. Fattori, and J. Williams, Adv. Mater. **19**, 4000 (2007).

[29] C.-C. Wu, Y.-T. Lin, K.-T. Wong, R.-T. Chen, and Y.-Y. Chien, Adv. Mater. **16**, 61 (2004).

[30] Lunt *et al.* (Ref. 12) measured the diffusion length of singlet excitons in N,N'-di(naphthalen-2-yl)-N,N'-diphenyl-benzidine (α-NPD) to (5.1 ± 1.0) nm, a material having similar properties as 4P-NPD (Ref. 7).

[31] K. Goushi, R. Kwong, J. J. Brown, H. Sasabe, and C. Adachi, J. Appl. Phys. **95**, 7798 (2004).

[32] Y. Kawamura, K. Goushi, J. Brooks, J. J. Brown, H. Sasabe, and C. Adachi, Appl. Phys. Lett. **86**, 071104 (2005).

[33] D. Berner, H. Houili, W. Leo, and L. Zuppiroli, *Physics of Organic Semiconductors*, edited by W. Brütting (Wiley-VCH Verlag GmbH & Co. KGaA, Weinheim, 2005).
[34] M. Kemerink, D. Charrier, E. Smits, S. Mathijssen, D. Leeuw, and R. Janssen, Appl. Phys. Lett. **93**, 033312 (2008).
[35] M. Baldo and M. Segal, Phys. Status Solidi A **201**, 1205 (2004).
[36] I. Tanaka, Y. Tabata, and S. Tokito, Phys. Rev. B **71**, 205207 (2005).
[37] S. Watanabe, A. Furube, and R. Katoh, J. Phys. Chem. A **110**, 10173 (2006).
[38] Y. Roichman and N. Tessler, Appl. Phys. Lett. **80**, 1948 (2002).
[39] C. Tanase, E. J. Meijer, P. W. M. Blom, and D. M. de Leeuw, Phys. Rev. Lett. **91**, 216601 (2003).